Cardiac-specific deletion of natriuretic peptide receptor A induces differential myocardial expression of circular RNA and mRNA molecules involved in metabolism in mice

BAOYING CHEN[1*], PAN CHANG[2*], XI SHEN[3*], XIAOMENG ZHANG[2], JING ZHANG[2], XIHUI WANG[2] and JUN YU[3]

[1]Imaging Diagnosis and Treatment Centre, Xi'an International Medical Centre Hospital; [2]Department of Cardiology, The Second Affiliated Hospital, Xi'an Medical University; [3]Clinical Experimental Centre, Xi'an International Medical Centre Hospital, Xi'an, Shaanxi 710100, P.R. China

Received April 21, 2020; Accepted October 8, 2020

DOI: 10.3892/mmr.2020.11688

Abstract. Atrial natriuretic peptide (ANP) and brain natriuretic peptide (BNP) are important biological markers and regulators of cardiac function. The natriuretic peptide receptor A (NPRA), also known as NPR1 or guanylyl cyclase A, binds ANP and BNP to initiate transmembrane signal transduction by elevating the intracellular levels of cyclic guanosine monophosphate. However, the effects and mechanisms downstream of NPRA are largely unknown. The aim of the present study was to evaluate the changes in the global pattern of mRNA and circular RNA (circRNA) expression in $NPRA^{-/-}$ and $NPRA^{+/+}$ myocardium. Differentially expressed mRNA molecules were characterised using Gene Ontology and Kyoto Encyclopedia of Genes and Genomes pathway analysis and were found to be primarily related to metabolic processes. Moreover, circRNA expression was also examined, and a possible competing endogenous RNA network consisting of circRNA, microRNA (miRNA), and mRNA molecules was constructed. The results of this study indicated that NPRA may play a role in cardiac metabolism, which could be mediated by circRNA through endogenous competition mechanisms. These findings may provide insight into future characterisation of various ceRNA network pathways.

Introduction

Atrial natriuretic peptide (ANP) and brain natriuretic peptide (BNP) are members of the NP family, a group of structurally similar but genetically distinct peptides that are involved in important processes, such as natriuresis, diuresis, vasodilation, and metabolic regulation (1). ANP and BNP act by binding to the natriuretic peptide receptor A (NPRA), also called NPR1 or guanylyl cyclase A. Activation of NPRA could elevate the levels of the second messenger cyclic guanosine monophosphate (cGMP), which, in turn, mediates physiological and pathophysiological processes through cGMP-dependent protein kinase (2). Thus, NPRA signalling represents a classical signalling pathway mediating the functions of various types of organs and tissues, including the heart and blood vessels. Importantly, weakened signals of NPs were observed in cardiometabolic diseases, which might represent molecular targets for novel therapeutic approaches. To date, however, the underlying mechanisms governing these phenomena remain unclear (3).

Circular RNA (circRNA) has long been considered to be the outcome of 'splicing errors' (4). However, with advances in high-throughput sequencing, circRNA is now recognised as a class of RNA produced by the alternative shearing of pre-mRNA (5). Because circRNA molecules lack free ends, they are resistant to exonucleases and can, as such, escape normal RNA degradation. These characteristics imply that circRNA molecules could serve many potential roles, possibly acting as transcription regulators (6), microRNA (miRNA) sponges, and protein sponges, thereby modulating various biological processes (7-11). Moreover, circRNA molecules may also play a critical role in several cellular functions that participate in the pathogenesis and progression of diseases. For example, it has been widely reported that circRNA is a key regulatory factor of cardiovascular diseases, such as myocardial infarction (12), atherosclerosis (13), cardiomyopathy (14), and cardiac fibrosis (15,16). The results of previous studies have suggested that circRNA molecules may represent new potential therapeutic targets and biomarkers for cardiovascular diseases (17,18).

To the best of our knowledge, the functional relationship between NPs and circRNA has not been documented. In the present study, the expression profile of circRNA and mRNA molecules in the myocardium of mice with cardiac-specific

Correspondence to: Professor Jun Yu, Clinical Experimental Centre, Xi'an International Medical Centre Hospital, 777 Xitai Road, Gaoxin, Xi'an, Shaanxi 710100, P.R. China
E-mail: pclamper@163.com

*Contributed equally

Key words: circular RNA, microRNA, mRNA, natriuretic peptide receptor, metabolism, myocardium

deletion of NPRA was examined, in order to characterise novel underlying mechanisms of heart disease induced by the inactivation of natriuretic signalling, based on circRNA networks.

Materials and methods

Generation of mice with cardiac-specific deficiency in NPRA. All experimental protocols included in this manuscript were approved by The Institutional Animal Care and Use Committee of Xi'an Medical University. The NPRA conditional knockout mouse model ($NprA^{flox/flox}$) was generated by the Shanghai Model Organisms Centre, Inc. This model was developed using the CRISPR/Cas9 system against the C57BL/6 mouse background, as previously described (19,20). An NprA donor vector containing flox sites flanking exon 2 of the NprA gene was constructed. Two single guide RNA (sgRNA) sites targeting intron 1 and intron 2 were transcribed *in vitro*. The sequences of the sgRNA target sites were 5'-GAGACGAGG ACCAAGACTGCAGG-3' and 5'-GCACAGGGGCCGTCT CATGCAGG-3'. The donor vector with two sgRNAs and Cas9 mRNA was microinjected into C57BL/6 fertilized eggs. F_0-generation mice with positive homologous recombination were identified by long PCR. The primers used for correct 5' homology arm recombination were 5'-GACTTCAAATCC CAGCTCACAACC-3' and 5'-CAAAGATCGAATGGAGCC CTGTGT-3'. The primers used for correct 3' homology arm recombination were 5'-TATCTTGCGGCCCTCTGACTG TAT-3' and 5'-ACTGGCCCTCCGTGGTTAGCA-3'. The identity of the PCR products were confirmed by sequencing. NprA flox heterozygous mice were obtained by mating F_0 generation mice with wild-type C57BL/6 mice. The genotypes of F_1-generation $NprA^{flox/flox}$ mice were identified using the same genotyping methods as F_0-generation mice.

To achieve tissue-specific deletion of the NPRA gene, $NprA^{flox/flox}$ mice were crossed with Myh6-Cre transgenic mice (Shanghai Model Organisms Centre, Inc.) to obtain $NprA^{flox/flox}$/Myh6-Cre mice. Both the $NPRA^{-/-}$ and $NPRA^{-/+}$ mice were identified by agarose gel electrophoresis and ethidium bromide staining (Fig. S1).

Isolation of myocardium. All mice were euthanised by inhaling oxygen with 5% isoflurane at a rate of 1 l/min. The mice were confirmed to be deeply anaesthetized if they were immobile for 1 min. A 25% volume of CO_2 gas was constantly flowed into the chamber to bring the mice to the point of clinical death, which was confirmed by cessation of the heartbeat and respiration. The hearts were subsequently removed to obtain the myocardium. Briefly, the cardiac tissue was isolated and placed in ice-cold PBS and all fat and connective tissue were removed. The samples were stored in -80˚C until use.

Reverse transcription-quantitative (RT-q) PCR validation. To measure cardiac mRNA expression of NPRA in mice, the myocardium samples (n=5 in each group) were collected and washed in PBS. Total RNA was then isolated from myocardium samples using TRIzol® (Thermo Fisher Scientific, Inc.) from myocardium samples. RNA concentration was then measured by the NanoDrop™ ND-1000 (NanoDrop™ Technologies; Thermo Fisher Scientific, Inc.). The RNA samples were reverse transcribed into cDNA using SuperScript™ III Reverse Transcriptase (Invitrogen; Thermo Fisher Scientific, Inc.). Briefly, the mixture contained RNA, Oligo $(dT)_{18}$ (Takara Bio, Inc.), Random 6 mers (Takara Bio, Inc.), dNTPs Mix (HyTest Ltd.), RNase free dH_2O and was placed in a 65˚C water bath for 5 min and on ice for 2 min. Following a short centrifugation in a palm centrifuge for 5-10 sec to make the mixture to gather at the bottom of the centrifuge tube, the RT reaction solution including 5X First-Strand Buffer (Invitrogen; Thermo Fisher Scientific, Inc.), DTT (Beijing Solarbio Science & Technology Co., Ltd.), RNase Inhibitor (Epicentre; Illumina, Inc.) and SuperScript™ III Reverse Transcriptase (Invitrogen; Thermo Fisher Scientific, Inc.) was sequentially added and the mixture was kept at 37˚C for 1 min. The solution was incubated at 50˚C for 60 min, then the reaction was terminated by incubation at 70˚C for 15 min. The cDNA obtained was diluted 1:10 and stored at -20˚C until use. qPCR was performed using TransStart™ SYBR Green qPCR Supermix (Takara Bio, Inc.) to determine the expression levels of NPRA. β-actin was included as an internal normalization reference gene for mRNA expression. All the PCR products were subjected to electrophoresis on a 2% agarose gel and visualized using ethidium bromide staining to confirm the presence of a single band of the expected size. The amplification efficiencies of qPCR for the target gene and the endogenous control were approximately equal and were calculated through a dilution series of cDNA. The qPCR reaction system included 2 μl cDNA, 5 μl 2C Master mix (Arraystar, Inc.) and 0.5 μl of each primer (10 μM solution) and diethylpyrocarbonate-treated water was added for a total volume of 10 μl. All qPCR reactions were performed in triplicate, including template-free controls. The thermocycling conditions consisted of an initial denaturation at 94˚C for 3 min, followed by 40 cycles of denaturation at 94˚C for 10 sec, and annealing at 56˚C 20 sec, then extension at 72˚C for 30 sec, and a final extension at 72˚C for 5 min The data were analysed using the comparative Cq ($\Delta\Delta$Cq) method (21).

To confirm the expression of differentially expressed genes (DEGs), including mRNAs and circRNAs, briefly, the sequences of candidate mRNAs and circRNAs were obtained from the CircInteractome database (http://circinteractome.nia.nih.gov/). The GAPDH and β-actin housekeeping genes were used as internal controls. The reverse transcription was performed as described above. The thermocycling conditions were as follows: i) Initial denaturation at 95˚C for 10 min; and ii) 40 cycles of denaturation at 95˚C for 10 sec, and annealing at 60˚C for 1 min. A melting curve analysis was performed after the amplification was complete by cooling the reaction to 60˚C and then heating slowly to 99˚C. The amplification products were analysed by 2% agarose gel electrophoresis and ethidium bromide staining. The relative quantification of the expression of the investigated genes was performed using a standard curve.

All primers were designed using Primer 5.0 and synthesized using a ViiA 7 Real-time PCR System (Applied Biosystems; Thermo Fisher Scientific, Inc.). Primer sequences are presented in Tables I and II.

Western blotting. For the preparation of tissue lysates, hearts from mice were dissected and washed with ice-cold PBS,

Table I. Reverse transcription-quantitative PCR primers used to confirm the expression of mRNAs.

Target genes	Primer sequences	Annealing temperature, ˚C	Product length, bp
β-actin (mouse)	F: 5' GCAGGAGTACGATGAGTCCG 3'		
	R: 5'ACGCAGCTCAGTAACAGTCC3'	60	247
NPRA	F: 5' GGCTGTGAAACGTGTGAACC 3'		
	R: 5' GTCGGTACAAGCTCCCACAA 3'	60	121
Rhobtb1	F: 5' AAAGCGCCAACCGTGAG 3'		
	R: 5' CTGCTTGGTGTAGAGGTATTCC 3'	60	83
Zbtb4	F: 5' CTGTGAGAAGGTGTTTGCCC 3'		
	R: 5' GCTCCCTGACTGTAGGTCTTGT 3'	60	279
Tfpi	F: 5' GATTCGTGTACGGTGGCT 3'		
	R: 5' GGCACTTTGGGAGACTGG 3'	60	199
S100a9	F: 5' TGGTGGAAGCACAGTTGG 3'		
	R: 5' TTGCCATCAGCATCATACAC 3'	60	135
Hp	F: 5' GAGGCAAGAGAGGTCCACGAT 3'		
	R: 5' CAAGTGCTCCACATAGCCGTT 3'	60	160
Cdkn1a	F: 5' TTGTCGCTGTCTTGCACTC 3'		
	R: 5' GTGGGCACTTCAGGGTTT 3'	60	159
Cbfa2t2	F: 5' GATGCCAACGGGCTCTAA 3'		
	R: 5' TGCTTCCTGCCAACTTCA 3'	60	138
Agpat2	F: 5' CAGATCGCCAAGCGTGAG 3'		
	R: 5' CCCATTGTCGTTGCGTGTA 3'	60	189
Nutf2	F: 5' AACCCAACTAGGCGCAATT 3'		
	R: 5' GCCGTGATGCTATGCTGAA 3'	60	132
Alg12	F: 5' AGGGCATATCTTGGTGAA 3'		
	R: 5' TCTTGTCATACCTCCAGTCA 3'	60	203
Gm20521	F: 5' CTTTGGTGGGACAAGTGC 3'		
	R: 5' TGTAGCTCCTTTAGCTTCTCA 3'	60	151
Gbp10	F: 5' TTGTTGGATGGTCCCGTACT 3'		
	R: 5' GTGATTCTGTCCCGCCAG 3'	60	62

F, forward; R, reverse; bp, base pair.

then homogenized with RIPA buffer (Beyotime Institute of Biotechnology) containing 150 mmol/l NaCl as previously described (22). Cell lysates were prepared for western blotting as previously described (23). Protein concentrations were determined using a BCA protein assay kit (Beyotime Institute of Biotechnology). After adjustment of protein concentration, the lysates were boiled in SDS loading buffer for 5 min then resolved by 10% SDS-PAGE and 20 μg of protein was loaded per lane. Gels were then transferred to an Immobilon-P PVDF membrane (EMD Millipore), which was blocked by 5% non-fat dried milk in TBST (Tris Buffer Saline with 0.1% Tween 20) buffer for 2 h at room temperature and incubated with primary antibodies against mouse NPRA (cat. no. LS-C264634; 1:500; LifeSpan BioSciences, Inc.) and GAPDH (cat. no. 2118, 1:1,000; Cell Signaling Technology, Inc.) in TBS + 0.1% Tween-20 (TBST) and 5% non-fat dry milk overnight at 4˚C. Membranes were subsequently washed in 5% milk/TBST and incubated with HRP-conjugated secondary antibody for 2 h at room temperature. Protein bands were visualised using a chemiluminescence detection kit (EMD Millipore).

RNA sequencing (RNA-seq). Total RNA from each sample was quantified by agarose gel electrophoresis and further verified and quantified by Nanodrop ND-1000 spectrophotometer (NanoDrop Technologies; Thermo Fisher Scientific, Inc.). Agarose electrophoresis was used to determine the integrity of total RNA samples. A total of 1-2 μg total RNA from each sample was used for RNA-seq library preparation. Briefly, rRNA was removed from the total RNA with a RiboZero Magnetic Gold kit (cat. no. MRZG12324; Epicentre; Illumina, Inc.). The rRNA-depleted samples were then prepared for sequencing using the KAPA-stranded RNA-Seq Library Prep kit for Illumina (cat. no. KK8400; Kapa Biosystems; Roche Diagnostics). The library preparation procedure included the following steps: i) RNA molecules fragmentation; ii) first strand cDNA synthesis by reverse transcription; iii) second-strand cDNA synthesis dUTP instead of dTTP (with no Uracil-DNA glycosylase treatment); iv) end repair and 3' adenylation of the double-stranded cDNA; v) ligation of the Illumina adapter; vi) PCR amplification; and vii) purification using magnetic beads (cat. no. KK8000; Kapa Biosystems; Roche Diagnostics).

Table II. Reverse transcription quantitative PCR primers used to confirm the expression of circRNAs.

Target genes	Primer sequences	Annealing temperature, ˚C	Product length, bp
β-actin (mouse)	F: 5' GTACCACCATGTACCCAGGC3' R: 5'AACGCAGCTCAGTAACAGTCC3'	60	247
GAPDH (mouse)	F: 5' CACTGAGCAAGAGAGGCCCTAT 3' R: 5' GCAGCGAACTTTATTGATGGTATT 3'	60	144
mmu_circRNA_43449	F: 5' CCTTCAGGGACAAAAAGGACAT 3' R: 5' CAGCTTATCCGTTGCTCCAAT 3'	60	159
mmu_circRNA_36265	F: 5' AGCAAGTCGGCAAAAGGC 3' R: 5' TCCACAGACACTGAAAGCTGAT 3'	60	129
mmu_circRNA_30261	F: 5' CTCACGCTACCCTACACTCTGG 3' R: 5' CACACACCTGGACACATCTGAAT 3'	60	85
mmu_circRNA_36266	F: 5' GAATAAAAACAAAAAGTTAGAGAAGC 3' R: 5' ATGAGATAAGAAATCAGGCCCT 3'	60	139
mmu_circRNA_32945	F: 5' TCTACCAGATCAACGTCCTCC 3' R: 5' CAGCACACATTTAAGCACCAG 3'	60	94
mmu_circRNA_22217	F: 5' AAGGAGGAAAAGCCCCAGACT 3' R: 5' GACATCAGAGAGCACACACCGT 3'	60	111
mmu_circRNA_005865	F: 5' GAAGCCAGGCTGTGTGTGTTA 3' R: 5' GGTGATTCTCTTGGACCCTTG 3'	60	84
mmu_circRNA_42481	F: 5' TGGCATGTACAGTTTCTGAGTTTT 3' R: 5' CTTGATGGAGGAGCAGGTTTG 3'	60	71
mmu_circRNA_19474	F: 5' AAAAACTCATTAATTGGGGTGGT 3' R: 5' CAGCCGTCACGCATCTCAT 3'	60	55
mmu_circRNA_19519	F: 5' TAGACCATTCCAGTTTCCACAG 3' R: 5' TTACACCCTTCAACCTACCCAT 3'	60	128
mmu_circRNA_19029	F: 5' ATGCCTGCTTCCTCAAAAACC 3' R: 5' TACCTTACCTGGAACCAAACTCTC 3'	60	134
mmu_circRNA_29619	F: 5' TGGTGGTGTTTGTGTCTGTGAT 3' R: 5' CATGACCAGTTCTTGGGCAGT 3'	60	108
mmu_circRNA_25320	F: 5' AAGAGAGTATAATGATTTTCTGGAAG 3' R: 5' TCCCACACTCAGGACAGTTTC 3'	60	103
mmu_circRNA_26033	F: 5' GGATGGCTTCAAAGTGTGTATT 3' R: 5' TCCTGTGATTCCACCTGTGC 3'	60	85

F, forward; R, reverse; circRNA, circular RNA; bp, base pair.

The quality of the libraries was evaluated using an Agilent 2100 Bioanalyzer, in order to check the concentration, the fragment size distribution (400-600 bp), and levels of adapter dimer contamination. The amount was quantified using the absolute qPCR method (24). For sequencing, the barcoded libraries were mixed in equimolar amounts. Sequencing was carried out using TruSeq SR Cluster kit v3-cBot-HS (150 cycles; paired end, cat. no. GD-401-3001; Illumina, Inc.) on an Illumina HiSeq 4000 platform according to the manufacturer's instructions. The sequencing data are available in the Gene Expression Omnibus (GEO) database (https://www.ncbi.nlm.nih.gov/geo) under accession no. GEO140678.

Bioinformatics analysis. As previously reported (25), image analysis and base calling were performed using the Off-Line Base Caller software v1.8 (Illumina, Inc.). Sequence quality was examined using FastQC software v0.11.7 (26). The cutadapt software (v1.2.1; http://code.google.com/p/cutadapt/) was then used to trim the fragments with a 5',3'-adaptor and to filter the reads ≤20 bp. The next step was alignment of the reads to the reference genome using Hisat 2 software (2.1.0; https://daehwankimlab.github.io/hisat2/) (27). The average reads was 35,871,134.2 and 88.9% of the clean reads were aligned. According to a previously published method (28), the transcript abundances were estimated with StringTie v1.3.3 (http://ccb.jhu.edu/software/stringtie/), and the number of identified genes and transcripts per group was calculated based on the mean of fragments per kilobase of exon model million reads mapped (FPKM) in each group, and the transcripts with FPKM ≥0.5 were retained. The ballgown R package v 3.5.0 (www.bioconductor.org/packages/release/bioc/html/ballgown.

html) was used to analyse the differentially expressed genes (DEGs) and transcripts by comparing the $NPRA^{-/-}$ group to the $NPRA^{+/+}$ group. The adjusted P-values of DEGs were obtained by multiple checking and correction using the Benjamini and Hochberg method (29). Filtering was based on an absolute fold change cut-off >1.5, adjusted P≤0.05 and mean FPKM ≥0.5. CPAT v1.2.4 (http://lilab.research.bcm.edu/cpat/) was then used to determine whether transcript sequences were coding or non-coding. Principal component analysis (PCA) and Pearson correlation analysis were carried out on gene expression levels. Hierarchical clustering, Gene Ontology (GO) (30), Kyoto Encyclopedia of Genes and Genomes (KEGG) (31) pathway, scatter plot and volcano plot analysis were performed with the differentially expressed genes in the R v3.5.0 (http://www.r-project.org/), Python v2.7 or shell environment for statistical computing and graphics.

circRNA array analysis. Total RNA from the samples of both groups was quantified. As described previously (32,33), sample preparation and microarray hybridization were performed according to the manufacturer's protocols (Arraystar, Inc.). Briefly, total RNA from each sample was digested with RNase R (Epicentre, Inc.) to remove linear RNA. The resulting circRNA-enriched samples were then amplified and labelled with fluorescently labelled nucleotides using an Arraystar Super RNA labeling kit (Arraystar, Inc.) utilizing a random priming method according to Arraystar Super RNA labeling protocol. The labelled circRNA molecules were hybridized to the Arraystar Mouse circRNA Array v2 (8x15 K, Arraystar). Microarray slides were scanned with a G2505C Agilent Scanner (Agilent Technologies, Inc.).

The array images were analysed by Agilent Feature Extraction software (version 11.0.1.1; Agilent Technologies, Inc.). Quantile normalization and subsequent data processing were performed using with the limma package (version 3.11; https://bioconductor.org/packages/release/bioc/html/limma.html). Differentially expressed circRNA molecules (DE-circRNAs) with statistical significance in expression levels between the two groups were identified using a volcano plot. The circRNAs that were differentially expressed between the two groups were filtered by fold change filtering (FC>2). Hierarchical clustering was subsequently conducted to illustrate the distinguishable circRNA expression profiles among samples. The raw data of microarray data are available in the GEO (https://www.ncbi.nlm.nih.gov/geo/) under accession no. GSE140798.

Prediction of circRNA-miRNA-mRNA network. As described previously (34,35), the circRNA-miRNA interaction was predicted using the Arraystar miRNA target prediction software (version 1.0, Arraystar Inc.) based on TargetScan44 and miRanda, and the DE-circRNAs were annotated in detail with circRNA-miRNA interaction information. TargetScan (version 7.2; http://www.targetscan.org/), miRanda (http://www.microrna.org/), and miRDB (http://www.mirdb.org/) were used to predict the microRNA-mRNA interactions that match the seed region of mouse miRNA sequences obtained from miRBase (http://www.mirbase.org/). In addition, if a miRNA molecule could bind to both the circRNA and target mRNA, the targeted circRNA was defined as a candidate competing endogenous RNA (ceRNA) for the gene, and the circRNA-miRNA-mRNA interactions thus represent candidate ceRNA pairs (circRNA connected with miRNA and miRNA connected with mRNA). In addition, circRNA and genes in candidate ceRNA pairs are required to have the same direction of change of expression level (upregulation or downregulation) in DEG analysis because of a positive correlation in the expression of ceRNA pairs (36). Then, the DE-circRNAs and differentially expressed mRNA transcripts (DE-mRNAs) that were validated by RT-qPCR were included within the ceRNA network, while all others were excluded. The circRNA-miRNA-mRNA interaction network was constructed and visually displayed using Cytoscape (version 3.8.1; http://www.cytoscape.org/) based on the data analysis results.

Statistical analysis. Statistical analysis was performed using R statistical package (37) (v3.5.0; http://www.R-project.org/), SPSS v19.0 (SPSS, Inc.) and Prism 6 (GraphPad Software). A total of five samples were included in each group. DEGs and DE-circRNAs were obtained by comparing the $NPRA^{-/-}$ group and the $NPRA^{+/+}$ group. Student's t-test was used to obtain P-values. The adjusted P-values of DEGs were obtained by multiple checking and correction based on the Benjamini and Hochberg method (29). Filtering was based on absolute FC >1.5 in DEGs and FC >2 in DE-circRNAs, adjusted P-value ≤0.05 and mean FPKM ≥0.5 were employed for filtering. RT-qPCR, statistical significance was assessed with Student's t-test. Data are presented as the mean ± SEM of three experimental repeats. P<0.05 was considered to indicate a statistically significant difference.

Results

NPRA was specifically knocked out in the myocardium of mice. To obtain a Cre recombinase-mediated, loxP-directed deletion of the NprA gene, a targeting construct was designed in which the second exon of NprA was flanked by two loxP sites (Fig. 1A). In $NprA^{flox/flox}$/Myh6-Cre mice the NPRA gene was specifically disrupted in the myocardium. Following Cre recombination, exon 2 of NprA was deleted, leading to gene reading frame transcoding and protein function loss. The loss of cardiac expression of NprA was determined by RT-qPCR (Fig. 1B) and western blotting (Fig. 1C). Homozygous knockout ($NPRA^{-/-}$) and heterozygous ($NPRA^{-/+}$) mice were identified by PCR genotyping and agarose gel electrophoresis staining (Fig. S1).

Differentially expressed mRNAs associated with metabolic processes are present in cardiac-specific $NPRA^{-/-}$ mice. The transcriptional profiles of $NPRA^{-/-}$ and $NPRA^{+/+}$ mice were determined using RNA-seq. The resulting scatter plot (Fig. 2A), volcano plot (Fig. 2B), and hierarchical clustering map (Fig. 2C) highlighted significant (DEGs) between $NPRA^{-/-}$ and $NPRA^{+/+}$ mice (n=5 in each group). Scatter plots are commonly used to display differences in gene expression between two datasets and to assess trends in population distribution. The values corresponding to the x and y-axes in the scatter plot are the normalized, $\log_2$-scaled FPKM of $NPRA^{+/+}$ and $NPRA^{-/-}$ mice, respectively. Symbols above the upper

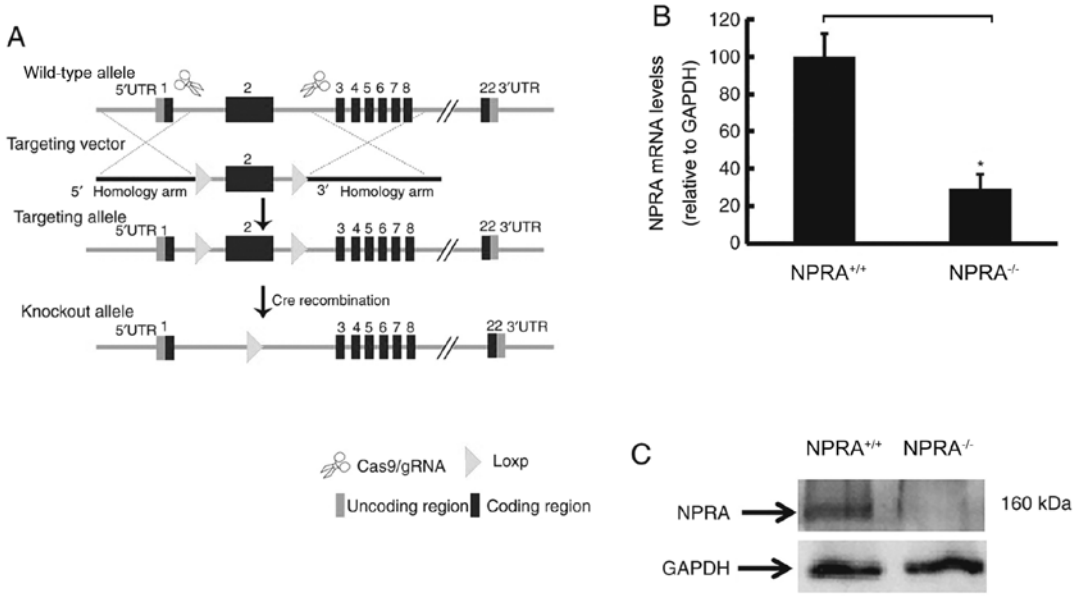

Figure 1. Specific NPRA knock out in murine myocardium. Generation of mice with cardiac-specific deletion of NPRA. (A) Partial schematic map of the murine NPRA gene locus, the targeting vector, the targeted recombinant allele, and the Cre recombination-generated deletion. (B) mRNA expression of NPRA was verified using reverse-transcription quantitative PCR. Data are presented as the mean ± SEM. *P<0.05 vs. NPRA$^{+/+}$. (C) NPRA protein was detected by western blotting. NPRA, natriuretic peptide receptor; UTR, untranslated region; gRNA, guide RNA.

green line and below the lower green line indicate fold change >1.5 between the between NPRA$^{-/-}$ and NPRA$^{+/+}$ mice. The volcano plot displays the relationship between the fold change of each DEG and the associated P-value in each sample group. Data clusterisation successfully discriminated NPRA$^{-/-}$ from NPRA$^{+/+}$ samples. All 10 samples were included for further analysis. However, only very few of these genes were considered to be differentially expressed with an adjusted P<0.05 and fold change >1.5. Indeed, seven were upregulated, and nine were downregulated.

GO enrichment analysis was used to identify significantly enriched GO terms associated with the potential functional roles of DEGs through three categories: Biological process (BP), molecular function (MF), and cellular component (CC). Enriched terms with significant differences (P<0.05) were selected and ranked by enrichment score (-$\log_{10}$-scaled P-value). A total of 4 BP terms, 2 MF terms, and 11 CC terms were significantly enriched in NPRA$^{-/-}$ mice, relative to NPRA$^{+/+}$ mice (Fig. S2A). Intriguingly, 2 out of 4 significantly enriched BP terms were related to the 'lipid metabolic process' (Fig. 3A). In KEGG pathway analysis, only a single significant pathway, 'metabolic pathways', was observed (Fig. 3B).

Among the downregulated genes, 99 BP terms, 13 MF terms, and 11 CC terms were found by GO analysis (Fig. S2B). The top 10 BP terms in the NPRA-deficient group ranked by enrichment score are shown in Fig. 3C. Notably, three of the top 10 BP terms were related to 'metabolic process'. These three terms are regulation of cellular metabolic process (GO: 0031323), regulation of metabolic process (GO: 0019222) and negative regulation of metabolic process (GO: 0009892).

To validate the RNA-seq results and confirm the differential gene expression profile, a subset of 12 genes which involving with metabolic process terms we got in GO analysis, including Agpat12, Alg12, Cbfa2t2, Cdkn1a, Nutf2, Rhobtb1, S100a9, Tfpi, Zbtb4, Hp, Gbp10, and Gm20521, were selected out of all 16 DEGs, and their expressions were measured using RT-qPCR. Among these genes, Alg12, Cdkn1a, S100a9, Gbp10 and Gm20521 were significantly differentially expressed in NPRA$^{-/-}$ mice, compared with NPRA$^{+/+}$ mice (Fig. 4). Thus, these five genes were selected for subsequent experiments.

circRNA-miRNA-mRNA interaction network is activated to regulate cardiac metabolism under the condition of NPRA deletion. circRNA can act as a miRNA 'sponge' that regulates the expression of mRNA, and such circRNA-miRNA-mRNA interaction network plays important roles in the genesis and development of cardiovascular diseases (38). Therefore, it was hypothesized that a circRNA-miRNA-mRNA network might be at play in the context of cardiac-specific NPRA deletion, thus inducing metabolic dysfunction in the myocardium.

A murine circRNA microarray was used to analyse the circRNA profiles of the myocardium from NPRA$^{-/-}$ mice, compared with NPRA$^{+/+}$ mice. The normalized intensity for the NPRA$^{+/+}$ and NPRA$^{-/-}$ groups was nearly the same (Fig. 5A). DE-circRNA molecules between NPRA$^{-/-}$ and NPRA$^{+/+}$ mice are displayed in a hierarchical clustering map (Fig. 5D), as well as a scatter plot (Fig. 5B) and a volcano plot (Fig. 5C). Clusterisation successfully discriminated successfully discriminated NPRA$^{-/-}$ from NPRA$^{+/+}$ samples. In total, 55 upregulated and 197 downregulated DE-circRNAs were identified.

To further examine the regulatory mechanism underlying DEG profiles, all global changes in the expression pattern of circRNAs were predicted according to the complementary miRNA matching sequence. Using ceRNA analysis, a circRNA-miRNA-mRNA interaction network was constructed. To confirm the ceRNA network, the predicted circRNAs were compared to the DE-circRNAs profiles from the circRNA microarray, and the circRNAs involved in both the predicted circRNA profiles and DE-circRNA

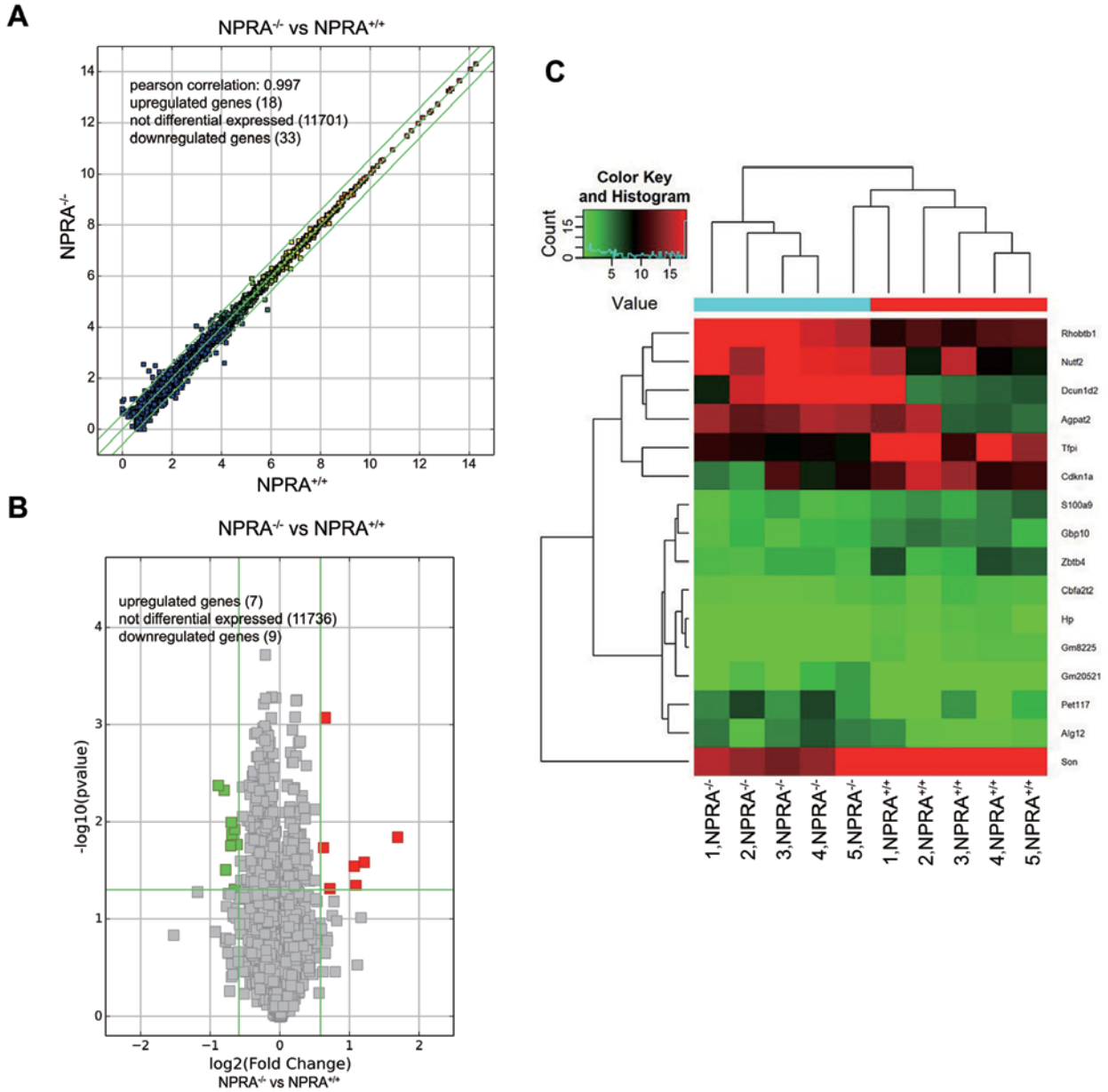

Figure 2. Scatterplot, volcano plot and hierarchical clustering of DEGs in NPRA$^{-/-}$ and wild-type mice. (A) Scatter plot for visual assessment of changes in the expression profiles of genes between NPRA$^{-/-}$ and NPRA$^{+/+}$ mice. The x- and y-axes represent the $\log_2$-scaled normalized FPKM of NPRA$^{+/+}$ and NPRA$^{-/-}$ mice, respectively. Dots above the top green line and below the bottom green line indicate an absolute fold change >1.5 between NPRA$^{-/-}$ and NPRA$^{+/+}$ mice. (B) Volcano plot. Red dots represent significantly upregulated genes; green dots represent significantly downregulated genes in cardiac tissues from NPRA$^{-/-}$ relative to NPRA$^{+/+}$ mice (absolute fold change >1.5 and P<0.05). The vertical lines indicate an absolute $\log_2$-scaled fold change of 1.5, thus representing the boundary of the differentially and non-differentially expressed genes. The horizontal line indicates P=0.05. (C) Heat map and hierarchical clustering analysis of DEGs from NPRA$^{-/-}$ and NPRA$^{+/+}$ mice. n=5 in each group. Green represents downregulation (NPRA$^{-/-}$ vs. NPRA$^{+/+}$). Red represents upregulation (NPRA$^{-/-}$ vs. NPRA$^{+/+}$). DEG, differentially expressed gene; NPRA, natriuretic peptide receptor.

profiles were selected for validation. In addition, because of a positive correlation in the expression of ceRNA pairs, candidate circRNAs were required to be oriented in the same direction direction of change of expression level in DEG analysis. Using this approach, 14 downregulated circRNAs (mmu_circRNA_005865, mmu_circRNA_19029, mmu_circRNA_19474, mmu_circRNA_19519, mmu_circRNA_22217, mmu_circRNA_25320, mmu_circRNA_26033, mmu_circRNA_29619, mmu_circRNA_30261, mmu_circRNA_32945, mmu_circRNA_36265, mmu_circRNA_36266, mmu_circRNA_42481 and mmu_circRNA_43449) were selected for validation by RT-qPCR. With RT-qPCR analysis, 6 circRNAs were significantly downregulated in the NPRA$^{-/-}$ mice, compared with NPRA$^{+/+}$ mice (Fig. 6).

Thus, the DE-circRNAs and DEGs that have been validated by RT-qPCR assay were included within the ceRNA network, and all others were excluded. Thus, with the majority of possible pathways excluded, only three target mRNA molecules (Alg12, Cdkn1a, and Gbp10) were included within the ceRNA network. The entire circRNA-miRNA-mRNA interaction network was constructed and visually displayed by Cytoscape. The top five miRNA binding sites predicted by ceRNA analysis for the six validated circRNAs in the ceRNA

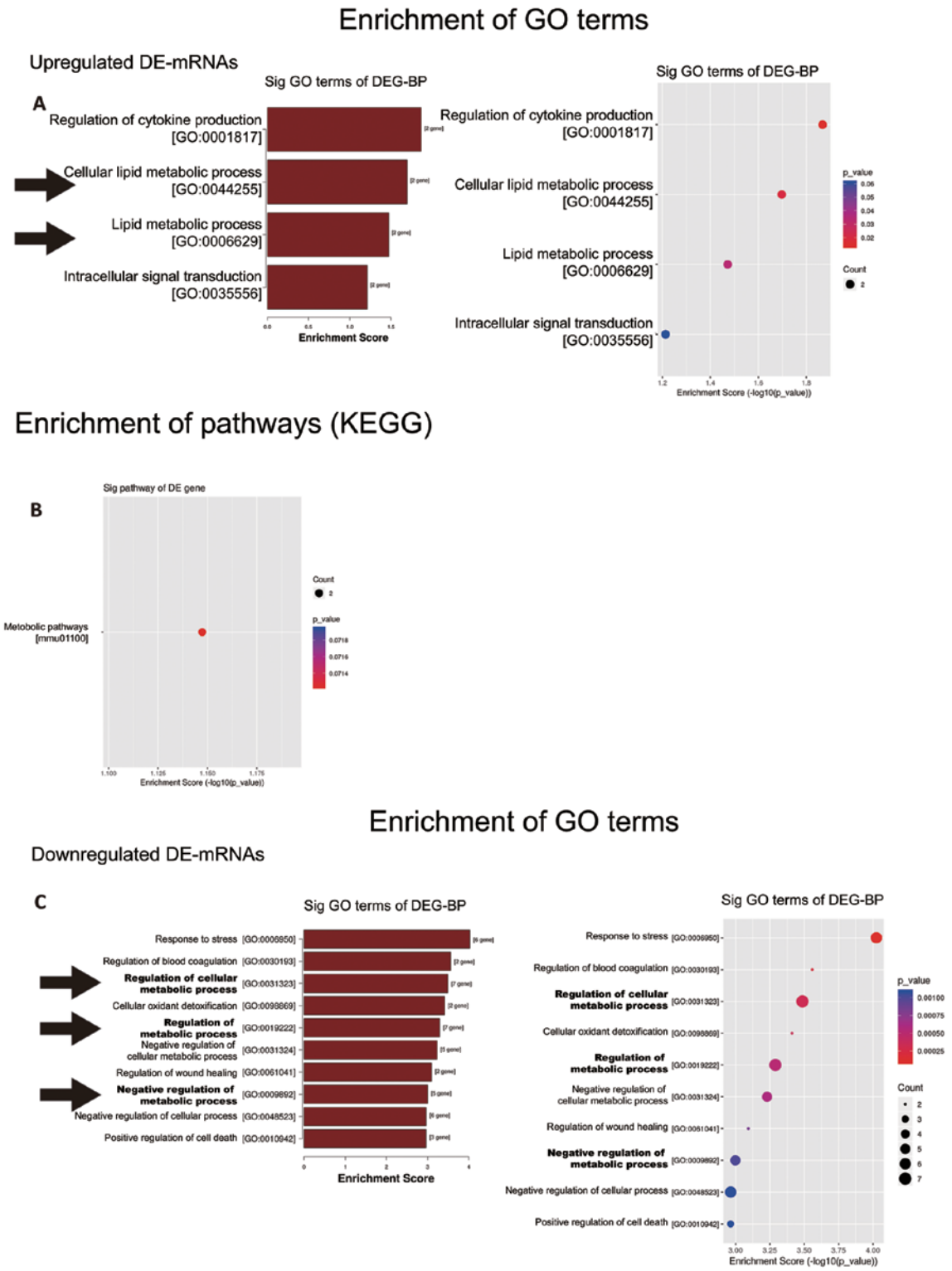

Figure 3. Differentially expressed mRNAs associated with metabolic processes were identified in cardiac-specific NPRA$^{-/-}$ mice. GO and KEGG pathway analysis of DEGs. (A) GO analysis of upregulated genes and BP terms showing the top four terms ranked by enrichment score. The enrichment score is indicated on the x-axis. The y-axis shows the names of GO terms. On the left graph, the arrows indicate terms associated with metabolism. On the right graph, the color scale represents the P-value. (B) KEGG pathway analysis of DEGs. Only one gene was identified and presented in a dot plot. The enrichment score is indicated on the x-axis. The y-axis shows the name of the KEGG pathways. The color scale represents the P-value (C) GO analysis of downregulated genes and BP terms showing the top 10 terms ranked by enrichment score. The enrichment score is indicated on the x-axis. The y-axis shows the names of GO terms. On the left graph, the arrows indicate terms associated with metabolism. On the right graph, the color scale represents the P-value. Sig, significant; GO, Gene Ontology; KEGG, Kyoto Encyclopedia of Genes and Genomes; BP, biological process.

network are presented in Table III. The top 5 predicted miRNA response elements (MREs) in the 3' UTR for each validated circRNA are presented in Fig. S3.

A circRNA-miRNA-mRNA interaction network was constructed, which included three genes (Alg12, Cdkn1a, and Gbp10) and six circRNAs (mmu_circRNA30261,

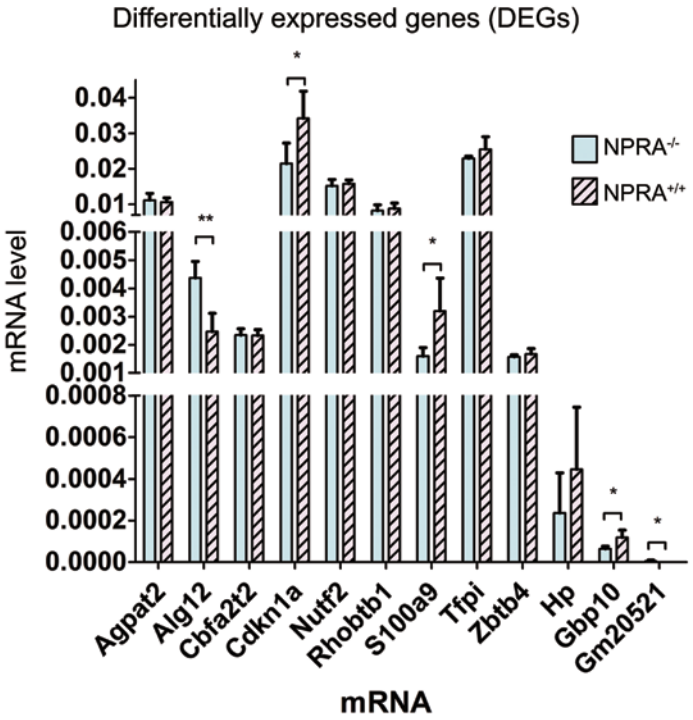

Figure 4. Validation of the RNA sequencing expression profiles of 12 genes selected from DEGs by RT-qPCR. To validate the results of RNA sequencing and confirm the differential gene expression profile, the expression levels of 12 genes out of all 16 DEGs were measured in NPRA$^{-/-}$ and NPRA$^{+/+}$ mice using RT-qPCR. *P<0.05, **P<0.01. Data are presented as the mean ± SEM. DEG, differentially expressed gene; NPRA, natriuretic peptide receptor; RT-qPCR, reverse transcription-quantitative PCR.

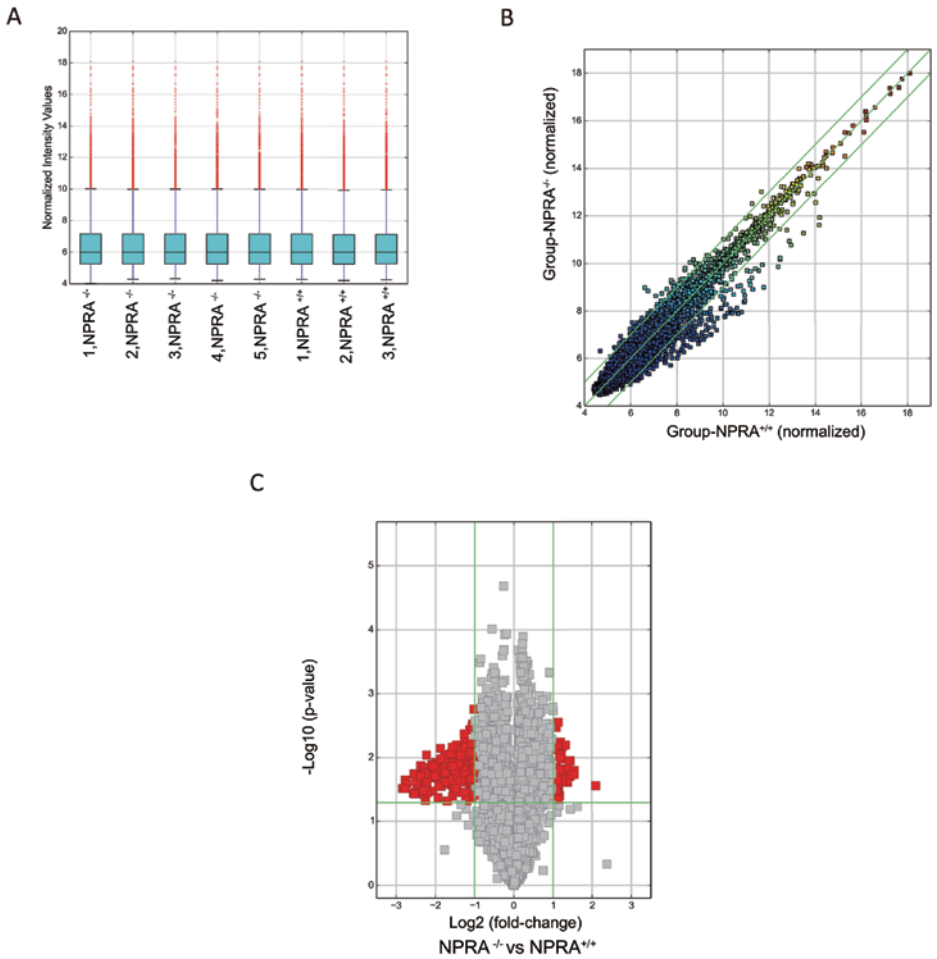

Figure 5. Continued.

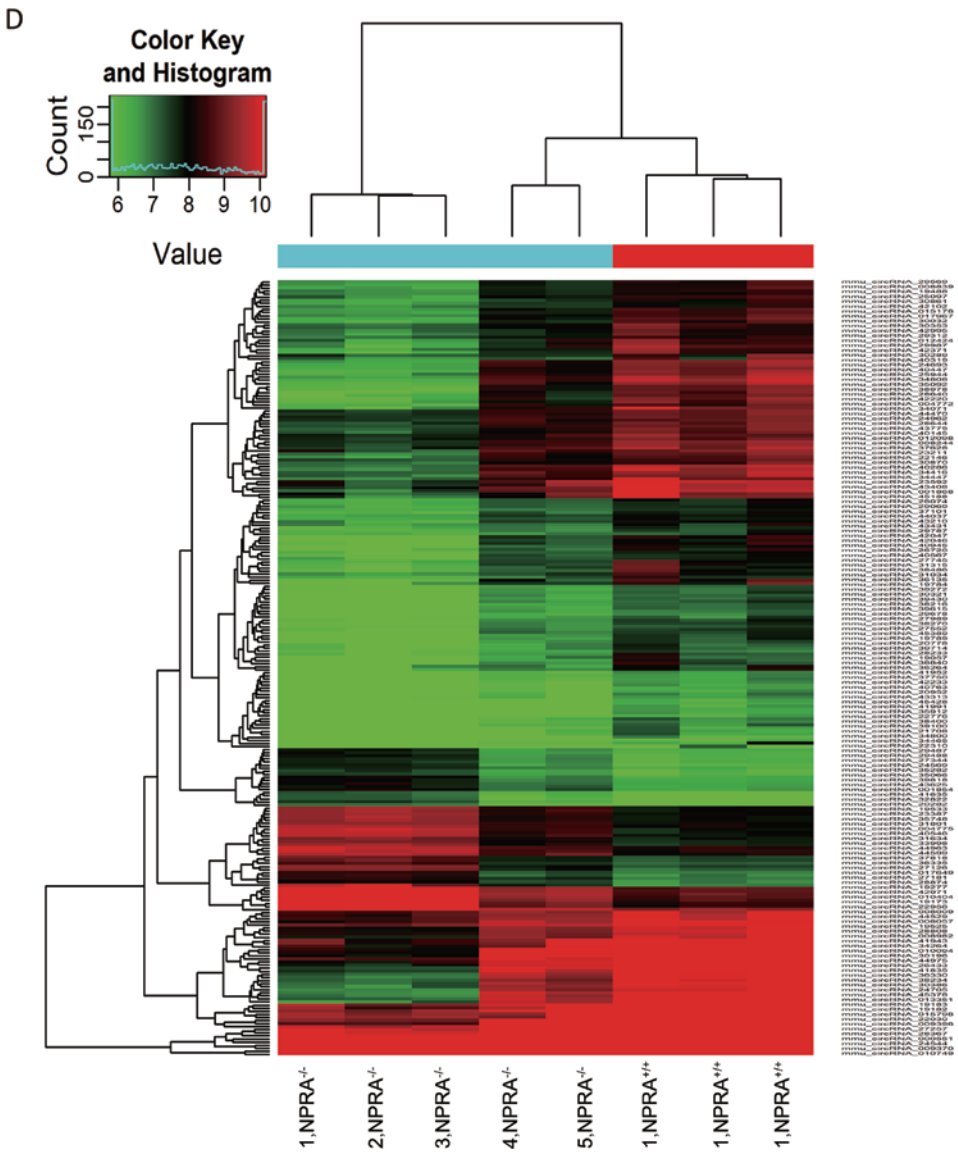

Figure 5. Scatterplot, volcano plot and hierarchical clustering of DE-circRNAs in NPRA$^{-/-}$ and NPRA$^{+/+}$. Microarray information of differential circRNA profiles from NPRA$^{-/-}$ or NPRA$^{+/+}$ myocardium. In total, 55 upregulated and 197 downregulated DE-circRNAs were identified (absolute fold change, >2; P<0.05). (A) Boxplots indicating the normalized intensity of the NPRA$^{-/-}$ or NPRA$^{+/+}$ groups. (B) Scatter plot for visual assessment of changes in the expression profiles of circRNAs between NPRA$^{-/-}$ and NPRA$^{+/+}$ mice. The x- and y-axes represent the $\log_2$- scaled normalized signal values of NPRA$^{+/+}$ and NPRA$^{-/-}$ mice, respectively. Dots above the top green line and below the bottom green line indicate an absolute fold change >1.5 between NPRA$^{-/-}$ and NPRA$^{+/+}$ mice. (C) Volcano plot of $\log_2$-scaled fold change on the x-axis and $\log_{10}$ P-values on the y-axis. The vertical lines indicate an absolute $\log_2$-scaled fold change of 1.5, thus representing the boundary of the differentially and non-differentially expressed genes. The horizontal line indicates P=0.05. The red symbols in the plot represent circRNAs that were significantly differentially expressed. (D) Hierarchical clustering analysis of circRNA expression data with absolute fold change >2.0 and P<0.05. Red and green colors indicated high and low expression, respectively and samples are divided into different groups naturally. NPRA, natriuretic peptide receptor; DE, differentially expressed; circRNA, circular RNA.

mmu_circRNA43449, mmu_circRNA36266, mmu_circRNA32945, mmu_circRNA42481, and mmu_circRNA29619). Moreover, 162 miRNAs were predicted in this network (Fig. 7; Table IV). This network may provide insight into the potential interactions between circRNA candidates and their target genes.

Discussion

The present study suggested that deficiency in NP signalling may result in metabolic dysfunction involving a circRNA-miRNA-mRNA interaction network. This conclusion is based on the following findings: i) The expression profiles of mRNA and circRNA molecules were different between the NPRA$^{-/-}$ and the NPRA$^{+/+}$ mice; ii) GO analysis demonstrated that DEGs were associated with BP terms related to metabolism, especially 'lipid metabolic processes'; iii) KEGG analysis also revealed a single 'metabolic pathway'; and iv) a circRNA-miRNA-mRNA interaction network involved with cardiac metabolism was constructed by ceRNA analysis.

NPs are a group of peptide hormones that are mainly secreted from the heart and signal through c-GMP-coupled receptors (39). The most well-known biological functions of NPs are their renal and cardiovascular functions, reducing arterial blood pressure, as well as sodium reabsorption. Recently, a number of studies have indicated that NPs may play a

Table III. Top five miRNA binding elements for validated circRNAs.

CircRNA	MRE1	MRE2	MRE3	MRE4	MRE5
mmu_circRNA_29619	mmu-miR-1231-5p	mmu-miR-449a-5p	mmu-miR-6905-5p	mmu-miR-493-3p	mmu-miR-7034-3p
mmu_circRNA_30261	mmu-miR-185-3p	mmu-miR-5120	mmu-miR-669e-5p	mmu-miR-3100-3p	mmu-miR-7048-5p
mmu_circRNA_32945	mmu-miR-8100	mmu-miR-5110	mmu-miR-1966-5p	mmu-miR-6405	mmu-miR-6987-5p
mmu_circRNA_42481	mmu-miR-3098-3p	mmu-miR-683	mmu-miR-7069-5p	mmu-miR-3552	mmu-miR-6990-3p
mmu_circRNA_36266	mmu-miR-103-1-5p	mmu-miR-103-2-5p	mmu-miR-335-3p	mmu-miR-107-5p	mmu-miR-6400
mmu_circRNA_43449	mmu-miR-7092-3p	mmu-miR-1187	mmu-miR-466f	mmu-miR-669a-5p	mmu-miR-669p-5p

circRNA, circular RNA; MRE, miRNA response elements; miR, microRNA.

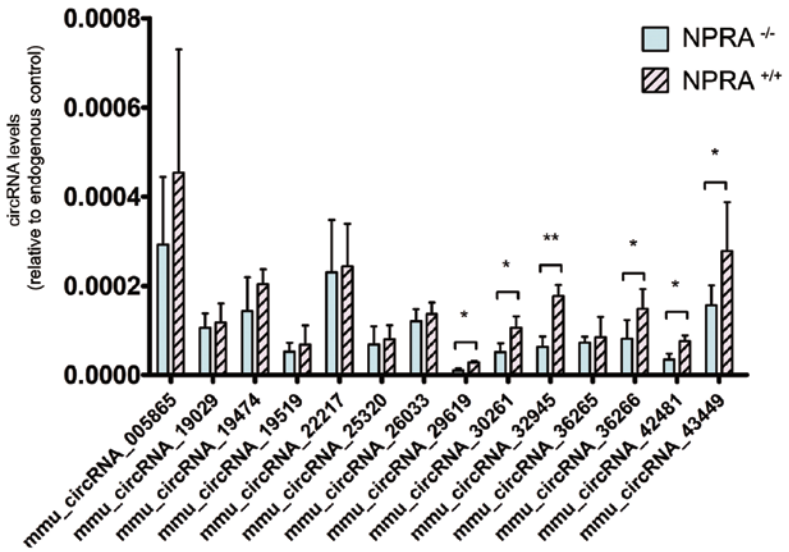

Figure 6. Reverse transcription-quantitative PCR validation of DE-circRNAs. A total of 14 DE-circRNAs were selected by fold-change values (FC>2) and P-values (P<0.05) for validation. *P<0.05, **P<0.01. Data are presented as the mean ± SEM. NPRA, natriuretic peptide receptor; DE, differentially expressed; circRNA, circular RNA.

pivotal role in metabolic functions, including the activation of lipolysis, lipid oxidation, and mitochondrial respiration (3,40). Despite high circulating concentrations of immunoreactive peptides, functional natriuretic peptide deficiency is observed in type-2 diabetes mellitus and cardio-metabolic complications, suggesting the involvement of weakened NP signalling in the pathophysiology of metabolic disorders (41). The presence of an NP deficiency often occur with metabolic disease, this phenomenon is generally accepted, as acknowledged by large cohorts (although challenged by some smaller cohorts), but the cause has not been fully elucidated (42). However, to the best of our knowledge, no previous study has investigated the expression of mRNAs in NPRA-deficient mice. In this study, using RNA-seq, the differential expression of mRNA transcriptional profiles between NPRA$^{-/-}$ myocardium and wild-type myocardium was determined. The differential expression of mRNA determined a profile of possible effectors downstream of the NPRA/cGMP signalling pathway. Notably, the number of DEGs was relatively low. Moreover, the results from GO analysis identified genes associated with metabolism. Similarly, although KEGG enrichment analysis only obtained a single pathway, it also clearly pointed to metabolic pathways, indicating that NP deficiency may play a pivotal role in metabolic disease.

Recent studies and developments in genome-wide analyses and RNA-seq technologies have demonstrated that small non-coding RNA molecules, such as miRNAs, linear long noncoding RNAs (lncRNAs) and circRNAs, can function in the regulation of biological processes (43,44). circRNA molecules are genetic products that are generated by back-splicing of a single pre-mRNA transcript (17). A growing number of circRNA molecules have been identified, and their

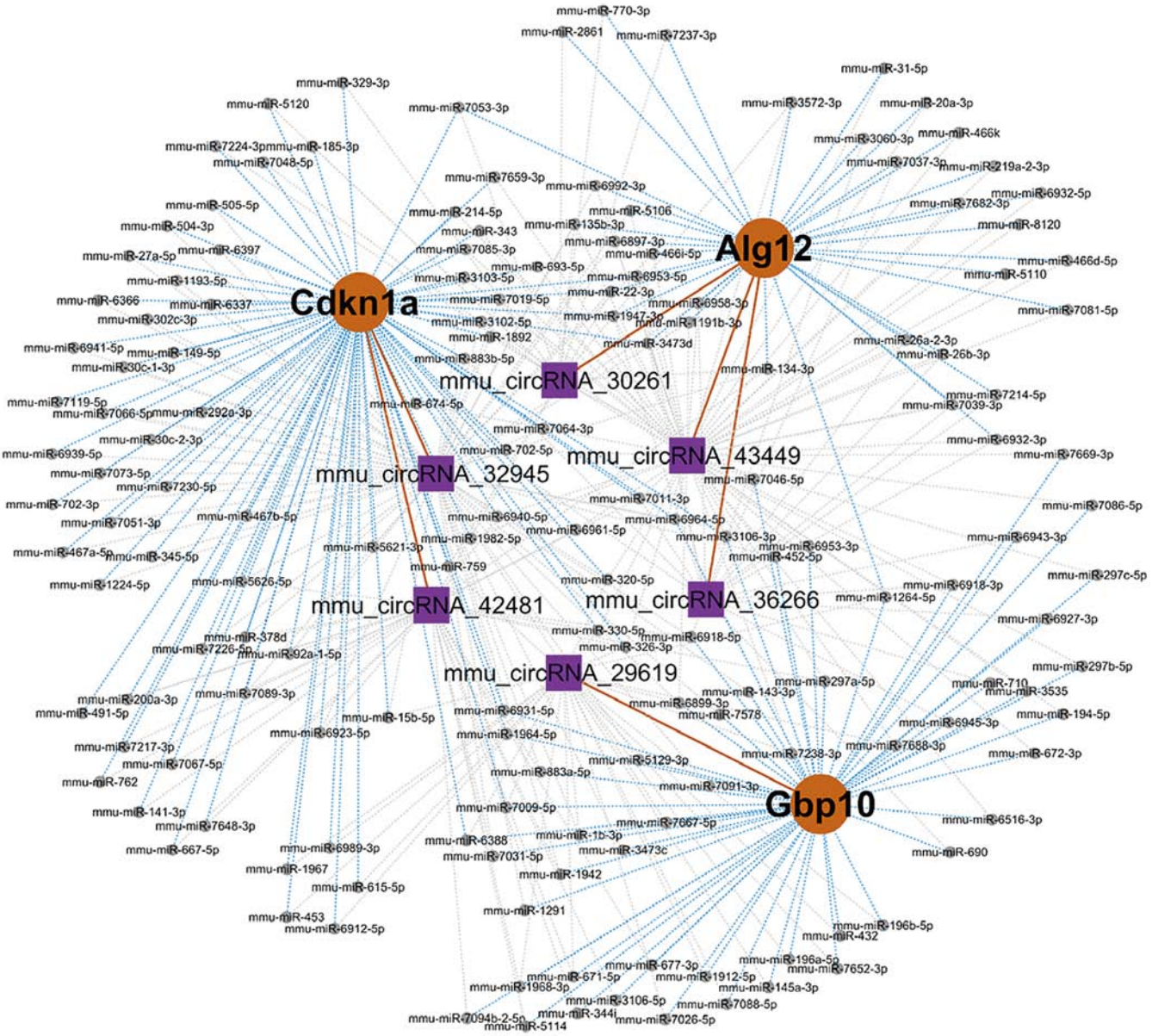

Figure 7. circRNA-miRNA-mRNA interaction network. A circRNA-miRNA-mRNA interaction network was constructed by ceRNA analysis. The ceRNA relationship pairs included six circRNAs as the core nodes, as well as 162 target miRNAs and three target mRNAs. Purple symbols represent circRNAs, while the orange nodes are the targeted genes. The grey nodes represent the predicted miRNAs. The dashed lines with blue colour represent mRNA-directed relationships, the dashed lines with grey colour represent circRNA-directed relationships, and the solid orange lines represent undirected relationships (ceRNA relationship). ceRNA, competing endogenous RNA; circRNA, circular RNA; miRNA/miR, microRNA.

pathophysiological functions have been determined. In particular, it has been demonstrated that circRNA are involved in cardiovascular disease initiation and progression, including atherosclerosis, cardiomyopathy, myocardial infarction, and cardiac fibrosis (17). In the present study, to determine whether the NPRA-related cardiometabolic profile (a term to describe a group of metabolic factors in cardiac associated with cardiovascular disease, metabolic syndrome and type II diabetes) (45) is associated with circRNAs, high-throughput screening of the DE-circRNAs was carried out using circRNA microarray analysis. To the best of our knowledge, the present study the first to use circRNA microarray analysis in NPRA$^{-/-}$ and NPRA$^{+/+}$ mice. A total of 55 significantly upregulated circRNAs and 197 significantly downregulated circRNAs were identified. Thus, deficiency in NP signalling resulted in altered expression of circRNAs, suggesting that circRNA molecules might represent important downstream effectors of NPRA/cGMP signalling. However, the underlying mechanism governing this phenomenon warrants requires further study.

Functionally, cytoplasmic circRNAs act as miRNA sponges by binding to miRNAs as competing endogenous RNAs (ceRNAs); according to the ceRNA hypothesis, the expression of cirRNA and miRNA should be negatively correlated (46). In the study, a circRNA-miRNA-mRNA network was constructed. Each circRNA and its potential complementary binding miRNAs were illustrated by the network, and specific interactions, such as mmu_circRNA_32945/mmu-miR-5626-5p/Alg12 were identified in the ceRNA network. Three genes, including

Table IV. Details of the ceRNA network.

Gene symbol	CeName	CeSymbol	CeType	Common miRNAs
Cdkn1a	mmu_circRNA_32945	mmu_circRNA_32945	circRNA	mmu-miR-1193-5p, mmu-miR-1224-5p, mmu-miR-149-5p, mmu-miR-15b-5p, mmu-miR-1892, mmu-miR-22-3p, mmu-miR-27a-5p, mmu-miR-292a-3p, mmu-miR-302c-3p, mmu-miR-30c-1-3p, mmu-miR-30c-2-3p, mmu-miR-3102-5p, mmu-miR-3103-5p, mmu-miR-320-5p, mmu-miR-345-5p, mmu-miR-378d, mmu-miR-467a-5p, mmu-miR-467b-5p, mmu-miR-504-3p, mmu-miR-505-5p, mmu-miR-5621-3p, mmu-miR-5626-5p, mmu-miR-6337, mmu-miR-6366, mmu-miR-6397, mmu-miR-6923-5p, mmu-miR-6931-5p, mmu-miR-6939-5p, mmu-miR-6941-5p, mmu-miR-6964-5p, mmu-miR-7019-5p, mmu-miR-702-3p, mmu-miR-702-5p, mmu-miR-7051-3p, mmu-miR-7064-3p, mmu-miR-7066-5p, mmu-miR-7073-5p, mmu-miR-7089-3p, mmu-miR-7119-5p, mmu-miR-7226-5p, mmu-miR-7230-5p, mmu-miR-883b-5p, mmu-miR-92a-1-5p
Alg12	mmu_circRNA_43449	mmu_circRNA_43449	circRNA	mmu-miR-1191b-3p, mmu-miR-135b-3p, mmu-miR-1947-3p, mmu-miR-20a-3p, mmu-miR-219a-2-3p, mmu-miR-26a-2-3p, mmu-miR-26b-3p, mmu-miR-31-5p, mmu-miR-3473d, mmu-miR-3572-3p, mmu-miR-466d-5p, mmu-miR-466i-5p, mmu-miR-466k, mmu-miR-5106, mmu-miR-5110, mmu-miR-6897-3p, mmu-miR-6932-3p, mmu-miR-6932-5p, mmu-miR-6953-5p, mmu-miR-6958-3p, mmu-miR-6992-3p, mmu-miR-7039-3p, mmu-miR-7081-5p, mmu-miR-7214-5p, mmu-miR-7682-3p, mmu-miR-8120
Cdkn1a	mmu_circRNA_42481	mmu_circRNA_42481	circRNA	mmu-miR-141-3p, mmu-miR-1964-5p, mmu-miR-200a-3p, mmu-miR-22-3p, mmu-miR-326-3p, mmu-miR-330-5p, mmu-miR-378d, mmu-miR-491-5p, mmu-miR-5626-5p, mmu-miR-667-5p, mmu-miR-6923-5p, mmu-miR-6940-5p, mmu-miR-6961-5p, mmu-miR-7011-3p, mmu-miR-7067-5p, mmu-miR-7089-3p, mmu-miR-7217-3p, mmu-miR-7226-5p, mmu-miR-762, mmu-miR-7648-3p, mmu-miR-92a-1-5p
Gbp10	mmu_circRNA_29619	mmu_circRNA_29619	circRNA	mmu-miR-1264-5p,mmu-miR-145a-3p, mmu-miR-1912-5p, mmu-miR-1968-3p, mmu-miR-196a-5p, mmu-miR-196b-5p, mmu-miR-1b-3p, mmu-miR-432, mmu-miR-6388, mmu-miR-671-5p, mmu-miR-6899-3p, mmu-miR-7009-5p, mmu-miR-7026-5p, mmu-miR-7088-5p, mmu-miR-7238-3p, mmu-miR-7652-3p, mmu-miR-7688-3p
Alg12	mmu_circRNA_30261	mmu_circRNA_30261	circRNA	mmu-miR-134-3p, mmu-miR-135b-3p, mmu-miR-2861, mmu-miR-3572-3p, mmu-miR-7053-3p, mmu-miR-7237-3p, mmu-miR-770-3p
Alg12	mmu_circRNA_36266	mmu_circRNA_36266	circRNA	mmu-miR-1947-3p, mmu-miR-26a-2-3p, mmu-miR-26b-3p, mmu-miR-3060-3p, mmu-miR-3473d, mmu-miR-6932-3p, mmu-miR-6953-5p, mmu-miR-6958-3p, mmu-miR-7037-3p, mmu-miR-7039-3p, mmu-miR-7214-5p

ceRNA, competing endogenous RNA; miR/miRNA, microRNA; circRNA, circular RNA.

Alg12, Cdkn1a, and Gbp10, were predicted to be associated with cardio-metabolic processes. In particular, Alg12 participates in asparagine N-linked glycosylation, metabolic pathways, metabolism of proteins, N-glycan biosynthesis and dolichyl-diphospho-oligosaccharide biosynthesis in both mice and humans (www.ncbi.nlm.nih.gov/gene/).

In conclusion, NP signalling plays an important role in the regulation of cardiac metabolism. The underlying mechanism governing this role involves a circRNA-miRNA-mRNA interacting network. This finding may provide insight into a possible novel pathway that is regulated by downstream signals of NPRA and modulates cardiac metabolism. The components of this network may represent candidate targets of cardiac metabolic disorders and warrant further investigation.

There were some limitations in the present study. First, the sample size in this study was small. Second, as circRNA may act as miRNA sponge, the circRNA-miRNA-mRNA networks were constructed. However, the molecular functions of the majority of identified circRNAs remain unknown, and several reports have shown that circRNAs can have multiple other functions, such as regulation of transcription, alternative splicing and translation (47). For this reason, functional experimental studies are still necessary to validate the roles played by these circRNAs in NPRA$^{-/-}$ myocardium. Also, further research should be designed and conducted to verify the validity of the whole of interaction network. For instance, this may include measurement of target gene expression, identification of circRNA molecules, pull-down assays with biotinylated circRNA probes, dual luciferase reporter gene experiments and other experiments for myocardial function and morphological changes, in order to examine the regulatory effect of NPs on cardiac function through this proposed ceRNA mechanism at the post-transcriptional level. Then whether one certain stable circRNA could formed by back splicing mechanism, whether one specific miRNA can be sponged by the circRNA, and certain target genes regulated by NPs will be identified. Future work should also focus on specific metabolic pathways and their regulation by NP signalling.

Acknowledgements

The authors thank Dr Jin-Song Chen (The Second Affiliated Hospital, Xi'an Medical University, Shaanxi, China) for his valuable suggestions for the present study.

Funding

The present study was supported by the National Natural Science Foundation of China (grant no. 81870172), the Shaanxi Provincial Key Research and Development Project (grant nos. 2018ZDXM-SF-068 and 2018SF-114), and Scientific Research Project of Xi'an Health Commission (grant no. 2020yb60).

Availability of data and materials

The sequence data were uploaded to the Gene Expression Omnibus database (https://www.ncbi.nlm.nih.gov/geo/). The GEO accession number is GEO: GSE140678. Microarray data were uploaded into the GEO database. The GEO accession number is GEO: GSE140798.

Authors' contributions

JY contributed to conception and design, funding acquisition and manuscript review. BC contributed to study design, provision of methodology and project administration. PC contributed to experimental operation and acquisition of data. XS contributed to data collection, statistical analysis, interpretation of data and manuscript preparation. XZ, JZ and XW contributed to formal analysis. All authors read and approved the final version of the manuscript.

Ethics approval and consent to participate

All experimental protocols included in this manuscript were approved by the Institutional Animal Care and Use Committee of Xi'an Medical University.

Patient consent for publication

Not applicable.

Competing interests

The authors declare that they have no competing interests.

References

1. Boerrigter G, Costello-Boerrigter LC and Burnett JC Jr: Natriuretic peptides in the diagnosis and management of chronic heart failure. Heart Fail Clin 5: 501-514, 2009.
2. Schipke J, Roloff K, Kuhn M and Mühlfeld C: Systemic, but not cardiomyocyte-specific, deletion of the natriuretic peptide receptor guanylyl cyclase A increases cardiomyocyte number in neonatal mice. Histochem Cell Biol 144: 365-375, 2015.
3. Cannone V, Cabassi A, Volpi R and Burnett JC Jr: Atrial natriuretic peptide: A molecular target of novel therapeutic approaches to cardio-metabolic disease. Int J Mol Sci 20: 3265, 2019.
4. Hsu MT and Coca-Prados M: Electron microscopic evidence for the circular form of RNA in the cytoplasm of eukaryotic cells. Nature 280: 339-340, 1979.
5. Ren S, Xin Z, Xu Y, Xu J and Wang G: Construction and analysis of circular RNA molecular regulatory networks in liver cancer. Cell Cycle 16: 2204-2211, 2017.
6. Jeck WR, Sorrentino JA, Wang K, Slevin MK, Burd CE, Liu J, Marzluff WF and Sharpless NE: Circular RNAs are abundant, conserved, and associated with ALU repeats. RNA 19: 141-157, 2013.
7. Hansen TB, Wiklund ED, Bramsen JB, Villadsen SB, Statham AL, Clark SJ and Kjems J: MiRNA-dependent gene silencing involving Ago2-mediated cleavage of a circular antisense RNA. EMBO J 30: 4414-4422, 2011.
8. Hansen TB, Jensen TI, Clausen BH, Bramsen JB, Finsen B, Damgaard CK and Kjems J: Natural RNA circles function as efficient microRNA sponges. Nature 495: 384-388, 2013.
9. Memczak S, Jens M, Elefsinioti A, Torti F, Krueger J, Rybak A, Maier L, Mackowiak SD, Gregersen LH, Munschauer M, *et al*: Circular RNAs are a large class of animal RNAs with regulatory potency. Nature 495: 333-338, 2013.
10. Ashwal-Fluss R, Meyer M, Pamudurti NR, Ivanov A, Bartok O, Hanan M, Evantal N, Memczak S, Rajewsky N and Kadener S: circRNA biogenesis competes with pre-mRNA splicing. Mol Cell 56: 55-66, 2014.
11. Guo JU, Agarwal V, Guo H and Bartel DP: Expanded identification and characterization of mammalian circular RNAs. Genome Biol 15: 409, 2014.

12. Huang S, Li X, Zheng H, Si X, Li B, Wei G, Li C, Chen Y, Chen Y, Liao W, *et al*: Loss of super-enhancer-regulated circRNA Nfix induces cardiac regeneration after myocardial infarction in adult mice. Circulation 139: 2857-2876, 2019.
13. Zhang F, Zhang R, Zhang X, Wu Y, Li X, Zhang S, Hou W, Ding Y, Tian J, Sun L and Kong X: Comprehensive analysis of circRNA expression pattern and circRNA-miRNA-mRNA network in the pathogenesis of atherosclerosis in rabbits. Aging (Albany NY) 10: 2266-2283, 2018.
14. Yang F, Li A, Qin Y, Che H, Wang Y, Lv J, Li Y, Li H, Yue E, Ding X, *et al*: A novel Circular RNA mediates pyroptosis of diabetic cardiomyopathy by functioning as a competing endogenous RNA. Mol Ther Nucleic Acids 17: 636-643, 2019.
15. Zhou B and Yu JW: A novel identified circular RNA, circRNA_010567, promotes myocardial fibrosis via suppressing miR-141 by targeting TGF-β1. Biochem Biophys Res Commun 487: 769-775, 2017.
16. Altesha MA, Ni T, Khan A, Liu K and Zheng X: Circular RNA in cardiovascular disease. J Cell Physiol 234: 5588-5600, 2019.
17. Bayoumi AS, Aonuma T, Teoh JP, Tang YL and Kim IM: Circular noncoding RNAs as potential therapies and circulating biomarkers for cardiovascular diseases. Acta Pharmacol Sin 39: 1100-1109, 2018.
18. Wang K, Long B, Liu F, Wang JX, Liu CY, Zhao B, Zhou LY, Sun T, Wang M, Yu T, *et al*: A circular RNA protects the heart from pathological hypertrophy and heart failure by targeting miR-223. Eur Heart J 37: 2602-2611, 2016.
19. Yang H, Wang H, Shivalila CS, Cheng AW, Shi L and Jaenisch R: One-Step generation of mice carrying reporter and conditional alleles by CRISPR/Cas-Mediated genome engineering. Cell 154: 1370-1379, 2013.
20. Feng GK, Ye JC, Zhang WG, Mei Y, Zhou C, Xiao YT, Li XL, Fan W, Wang F and Zeng MS: Integrin α6 targeted positron emission tomography imaging of hepatocellular carcinoma in mouse models. J Control Release 310: 11-21, 2019.
21. Livak KJ and Schmittgen TD: Analysis of relative gene expression data using real-time quantitative PCR and the 2(-Delta Delta C(T)) Method. Methods 25: 402-408, 2001.
22. Yu J, Bulk E, Ji P, Hascher A, Tang M, Metzger R, Marra A, Serve H, Berdel WE, Wiewroth R, *et al*: The EPHB6 receptor tyrosine kinase is a metastasis suppressor that is frequently silenced by promoter DNA hypermethylation in non-small cell lung cancer. Clin Cancer Res 16: 2275-2283, 2010.
23. Zhao HK, Chen BY, Chang R, Wang JB, Ni F, Yang L, Dong XC, Sun SH, Zhao G, Fang W, *et al*: Vasonatrin peptide, a novel protector of dopaminergic neurons against the injuries induced by n-methyl-4-phenylpyridiniums. Peptides 49: 117-122, 2013.
24. Lu Y, Xie L and Chen J: A novel procedure for absolute real-time quantification of gene expression patterns. Plant Methods 8: 9, 2012.
25. Wan QQ, Wu D and Ye QF: Candidate genes as biomarkers in Lipopolysaccharide-Induced acute respiratory distress syndrome based on mRNA expression profile by Next-Generation RNA-Seq analysis. Biomed Res Int 2018: 4384797, 2018.
26. Babraham Bioinformatics-FastQC A Quality Control tool for High Throughput Sequence Data.
27. Kim D, Langmead B and Salzberg SL: HISAT: A fast spliced aligner with low memory requirements. Nat Methods 12: 357-360, 2015.
28. Poole CJ, Lodh A, Choi JH and van Riggelen J: MYC deregulates TET1 and TET2 expression to control global DNA (hydroxy) methylation and gene expression to maintain a neoplastic phenotype in T-ALL. Epigenetics Chromatin 12: 41, 2019.
29. Benjamini Y and Hochberg Y: Controlling the false discovery rate: A practical and powerful approach to multiple testing. J R Stat Soc Ser B (Methodological) 57: 289-300, 1995.
30. Aebersold R and Mann M: Mass-spectrometric exploration of proteome structure and function. Nature 537: 347-355, 2016.
31. Kanehisa M, Furumichi M, Tanabe M, Sato Y and Morishima K: KEGG: New perspectives on genomes, pathways, diseases and drugs. Nucleic Acids Res 45: D353-D361, 2017.
32. He R, Liu P, Xie X, Zhou Y, Liao Q, Xiong W, Li X, Li G, Zeng Z and Tang H: circGFRA1 and GFRA1 act as ceRNAs in triple negative breast cancer by regulating miR-34a. J Exp Clin Cancer Res 36: 145, 2017.
33. Lv C, Sun L, Guo Z, Li H, Kong D, Xu B, Lin L, Liu T, Guo D, Zhou J and Li Y: Circular RNA regulatory network reveals cell-cell crosstalk in acute myeloid leukemia extramedullary infiltration. J Transl Med 16: 361, 2018.
34. Lin SP, Ye S, Long Y, Fan Y, Mao HF, Chen MT and Ma QJ: Circular RNA expression alterations are involved in OGD/R-induced neuron injury. Biochem Biophys Res Commun 471: 52-56, 2016.
35. Zhou J, Xiong Q, Chen H, Yang C and Fan Y: Identification of the spinal expression profile of non-coding rnas involved in neuropathic pain following spared nerve injury by sequence analysis. Front Mol Neurosci 10: 91, 2017.
36. Li JH, Liu S, Zhou H, Qu LH and Yang JH: StarBase v2.0: Decoding miRNA-ceRNA, miRNA-ncRNA and protein-RNA interaction networks from large-scale CLIP-Seq data. Nucleic Acids Res 42: D92-D97, 2014.
37. Team R: R Core Team. R A Language and Environment for Statistical Computing 2014. In: R Foundation for Statistical Computing, 2008.
38. Li M, Duan L, Li Y and Liu B: Long noncoding RNA/circular noncoding RNA-miRNA-mRNA axes in cardiovascular diseases. Life Sci 233: 116440, 2019.
39. Schlueter N, de Sterke A, Willmes DM, Spranger J, Jordan J and Birkenfeld AL: Metabolic actions of natriuretic peptides and therapeutic potential in the metabolic syndrome. Pharmacol Ther 144: 12-27, 2014.
40. Wu W, Shi F, Liu D, Ceddia RP, Gaffin R, Wei W, Fang H, Lewandowski ED and Collins S: Enhancing natriuretic peptide signaling in adipose tissue, but not in muscle, protects against diet-induced obesity and insulin resistance. Sci Signal 10: eaam6870, 2017.
41. Zois NE, Bartels ED, Hunter I, Kousholt BS, Olsen LH and Goetze JP: Natriuretic peptides in cardiometabolic regulation and disease. Nat Rev Cardiol 11: 403-412, 2014.
42. Verboven K, Hansen D, Jocken JWE and Blaak EE: Natriuretic peptides in the control of lipid metabolism and insulin sensitivity. Obes Rev 18: 1243-1259, 2017.
43. Ding B, Lou W, Xu L and Fan W: Non-coding RNA in drug resistance of hepatocellular carcinoma. Biosci Rep 38: BSR20180915, 2018.
44. Xuan L, Qu L, Zhou H, Wang P, Yu H, Wu T, Wang X, Li Q, Tian L, Liu M and Sun Y: Circular RNA: A novel biomarker for progressive laryngeal cancer. Am J Transl Res 8: 932-939, 2016.
45. Fernández-Cao JC and Doepking C: Role of ethnicity and environment on lifestyle and cardiometabolic profile in the Native American Mapuche population: Protocol for a systematic review and meta-analysis. Medicine (Baltimore) 97: e13354, 2018.
46. Salmena L, Poliseno L, Tay Y, Kats L and Pandolfi PP: A ceRNA hypothesis: The Rosetta Stone of a hidden RNA language? Cell 146: 353-358, 2011.
47. Wilusz JE: A 360° view of circular RNAs: From biogenesis to functions. Wiley Interdiscip Rev RNA 9: e1478, 2018.